

Theoretical modeling of prion disease incubation

R.V. Kulkarni¹, A. Slepoy², R.R.P. Singh¹, D.L. Cox¹, D. Mobley¹, and F. Pázmándi¹

¹*Department of Physics, University of California, Davis, CA 95616*

²*MS 0316, Sandia National Laboratories, P. O. Box 5800, Albuquerque, NM 87185-0316*

(November 2, 2018)

We present a theory for the laboratory and epidemiological data for incubation times in infectious prion diseases. The central feature of our model is that slow growth of misfolded protein-aggregates from small initial seeds controls the ‘latent’ or ‘lag’ phase, whereas aggregate-fissioning and subsequent spreading leads to an exponential growth or doubling phase. Such a general framework can account for many features of prion diseases including the striking reproducibility of incubation times when high doses are inoculated into lab animals. Furthermore, we explore the importance of aggregate morphology in determining the statistics of the incubation time. Broad incubation time distributions arise for low infectious dose, while our calculated distributions narrow to sharply defined onset times with increased dose. We use our distributions to obtain a fit for the experimental dose-incubation curves for distinct strains of scrapie and show how features of the dose-incubation curve, specifically (a) the logarithmic dose-dependence at high dose and (b) deviations from logarithmic behavior at low dose can be explained within our model. By fitting the experimental dose-incubation curves, we quantify our model parameters and make testable predictions for experiments which measure the time-course of infectivity. We apply our model to analysis of data from BSE epidemiology, iatrogenic CJD infections, and vCJD infections; these data are consistent with incubation times dominated by slow aggregation from a few seeds which are tens of nanometers in size. Within the model, small mammals derive shorter incubation times from much more rapid protein attachment rates which we suggest to arise from higher PrP^c concentrations that might be metabolically controlled. Further, based upon our analysis we suggest that vCJD incubation times are likely to be at the low end of previous estimates.

I. INTRODUCTION

Understanding the factors which regulate the incubation times for infectious prion diseases is important for assessing the risk of illness after potential exposure as well as for developing treatments which can delay disease onset. There are several striking aspects to prion disease incubation, which are not well understood: (i) The incubation times can run into years and decades [1], and yet, at the laboratory scale have been found to be highly reproducible. In fact, the reproducibility of incubation times with dose has been used as an independent measure of infectivity titre [2,3]. (ii) There seem to be distinct stages for the disease incubation after intracerebral inoculation: (a) Following rapid initial clearance, there is a ‘lag’ phase (also termed ‘zero’ phase [4,8]) during which there is little or no infectivity, and (b) an exponential growth or doubling phase, during which the infectivity increases exponentially with a well-defined doubling period [5–7]. Understanding the lag-phase is clearly important as any treatment strategy is more likely to succeed before the exponential growth phase takes over. (iii) As the dose of infection is increased in the laboratory, the incubation times become sharply defined and saturate to a dose independent value, but as the dose is reduced a broad distribution and a logarithmic dose dependence results [9]. Such a broad distribution has also been found in epidemiological studies of Bovine Spongiform Enceph-

elopathy (BSE) in England [10,11]. (iv) For infection across species, there is a ‘species barrier’ and the first passage takes considerably longer to incubate than subsequent passages [12,13]. (v) While prion aggregation has been observed *in vitro*, the aggregates are neuro-toxic but not infectious [14]. These are the issues which motivate our study.

The purpose of this paper is to test the extent to which a purely physico-chemical model can capture the main reproducible features of prion disease incubation. In particular, we emphasize the importance of the aggregate morphology in determining the statistics of incubation times. Our basic hypothesis is that the ‘lag phase’ is determined by growth of misfolded protein-aggregates from initial small seeds (acquired through infection) to a typical ‘fissioning dimension’, whereas subsequent aggregate-fissioning and spreading leads to exponential growth and the doubling phase. For a single seed, the lag phase develops a broad but well defined distribution, which we can calculate via a microscopic statistical model. Thus, when the infection is very dilute, there is a broad distribution of incubation times. At higher doses of infection, self-averaging due to independent growth from many seeds leads to sharply defined incubation times. The dose dependence and its saturation, as well as the ratio of lag time to doubling time depends on the morphology of the aggregates, *i.e.*, whether one has linear fibrils or compact higher-dimensional aggregates. In this sense, details of

incubation time distributions provide an indirect means to infer early growth morphologies. Alternative theoretical models which deal with the above issues have also been developed in the literature. [15–18,20,19,21]

The extent to which such a model explains the experimental phenomenology would help address the following questions: (i) *Are the incubation times dominated by the nucleation and growth of misfolded protein aggregates?* (ii) *Are the two phases of prion disease incubation, the lag phase and the exponential growth phase, controlled by the same process i.e. aggregation of misfolded proteins?* (iii) Assuming that aggregate growth controls the incubation time scales, we are led to ask: *What is the aggregate morphology during early growth and how does it influence the dose incubation curves* (iv) *Does current data inform us about the characteristic size of the aggregates?* (v) *What are the practical epidemiological impacts from our model incubation time distributions?* Can we use the model to constrain estimates of the number of infections of vCJD for example?

Employing statistical simulations of prion aggregation (based upon cellular automata rules) we argue here that several features of prion disease can be explained by exploring the statistics of the two phases of the disease incubation. Within our model, we show that compact two-dimensional aggregates can provide the observed broad distribution of incubation times for dilute doses and at the same time account for the typical large difference between lag time and doubling time. We present analytic calculations which provide a functional form for the distribution that can be used in further epidemiological studies, and we use these results to infer the dose dependence of the incubation time. Furthermore, our analysis shows how the dose-incubation curve can be related to experimental measurements of the time-course of infectivity and in particular, testable predictions can be made using our model for the dose dependence of the lag phase. Finally, we apply our model to epidemiological data for BSE (mad cow disease), iatrogenic CJD infections associated with *dura mater* transplants, and a vCJD cluster from the United Kingdom, from which we conclude that in all three cases the incubation time is dominated by slow aggregation from a few small (tens of nanometer scale) starting seeds. This size scale is comparable to small animals, but the estimated attachment rates are slower by an order of magnitude or more. We argue that the incubation time for vCJD is likely to be at the low end of previous estimates, implying an infectious toll in the hundreds rather than hundreds of thousands. We speculate that the differing attachment rate among species is regulated by the PrP^c concentration which in turn is metabolically controlled.

We organize our paper as follows: Section II discusses a model incubation time distribution, which illustrates how our basic picture relates to dose incubation curves in prion diseases. Sections III-V deal with microscopic

models related to protein misfolding, aggregation and fissioning. In Sections VI, VII, and VIII, we come back to the dose incubation curves, connections to epidemiological data and the disease phenomenology and discuss them in context of our models and present our conclusions.

II. A MODEL DISTRIBUTION AND DOSE INCUBATION CURVES

We first illustrate the ‘bare bones’ of our proposed picture for prion disease incubation by using a model distribution, where calculations can be done analytically. As mentioned in the previous section, the lag phase corresponds to aggregation of misfolded prions from the initial seed upto a ‘fissioning size’. This is a stochastic process and correspondingly there will be a distribution of aggregation times. Subsequent to this aggregation, we assume (based upon experimental observations) that the number of seeds increases exponentially with a well defined doubling time (t_2). This exponential growth continues until the number of seeds reaches a critical value which signals the onset of clinical symptoms and the end of the incubation period.

In this section, we assume the distribution of aggregation times from a single seed, $P(t)$, to be given by

$$P(t) = 0 \quad t < t_0 \quad (1)$$

$$= \frac{1}{n_1 t_2} \quad t_0 < t < t_0 + n_1 t_2 \quad (2)$$

$$= 0 \quad t > t_0 + n_1 t_2 \quad (3)$$

Here t_0 and n_1 are the parameters for the distribution. It has a sharp onset at time t_0 and its width is taken to be some multiple (n_1) of the doubling time t_2 . When there are many seeds present, each initial seed will start fissioning into two new seeds after an aggregation time according to the above distribution. We will assume that once a seed has fissioned once, it continues to fission or effectively double every t_2 time steps, which is independent of the above distribution. The microscopic basis for this assumption will be explained in section V. The incubation time is given by the mean time taken for a given initial number of seeds (D_i) to reach a critical number (D_f) following the above processes.

The dose dependence of the the incubation time is calculated through the following steps:

1) First we calculate the mean ‘first arrival’ time i.e. the mean time taken for the first aggregate fissioning event. Let the cumulative probability for the ‘first arrival’ time for D_i seeds be given by $F^{(D_i)}(t)$. Since each seed grows independently, this can be related to the cumulative probability for the ‘first arrival’ time for a single seed via the relation

$$F^{(D_i)}(t) = 1 - (1 - F^{(1)}(t))^{D_i} \quad (4)$$

The mean first arrival time t_1 is given by solving $F^{(D_i)}(t_1) = \frac{1}{2}$. For the simple probability distribution discussed above, the mean first arrival time is well-approximated by the expression

$$t_m(D_i) = t_0 + \frac{n_1}{2D_i}t_d \quad (5)$$

2) We now proceed to calculate the time spent in the doubling phase, *i.e.*, the time taken till the number of seeds reaches D_f . All the aggregates formed after fissioning are assumed to further fission in time t_2 . Besides these, initial seeds continue to ‘arrive’, *i.e.*, aggregate to the fissioning size and thus join the number seeds that are doubling. Let the number of such seeds ‘arriving’ in the time interval $m t_2 < t < (m + 1) t_2$ be given by $\alpha(m)D$. Then, $\alpha(m)$ is given by

$$\alpha(m) = F^{(1)}((m + 1)t_2) - F^{(1)}(mt_2) \quad (6)$$

3) For our model distribution, the above equation can now be used to calculate the mean incubation time, which is approximately given by

$$t_i = t_0 + \frac{n_1}{2D_i}t_2 + [\log_2(D_f) - \log_2(1 + \frac{D_i}{n_1})]t_2 \quad (7)$$

The above equation gives the dose-dependence of the incubation time for the model distribution. It should be noted that this expression already explains several generic features seen in experimental dose-incubation curves (DICs) and in the microscopic models we present in later sections. These are: 1) logarithmic dose-dependence at high doses and 2) deviations from logarithmic behavior at low doses. From the above expression for the incubation time, it can be seen that the dominant contribution to the incubation time at high D_i comes from the ‘doubling’ phase which gives a logarithmic dose-dependence. However at low doses ($D \leq n_1$), the time spent in the doubling phase does not change appreciably with dose. Instead, the variation in the incubation time comes from the dose-dependence of the ‘first arrival’ time *i.e.* the lag phase time. This is reflected as a deviation from the logarithmic behavior in the DIC which is seen in experimental DICs [22]. Our model thus makes the testable prediction that deviations from logarithmic behavior in the DIC should correspond to increases in the lag phase.

We now proceed to develop microscopic models for the initial aggregation process. The next section discusses the cellular automata approach to this problem.

III. CELLULAR AUTOMATA SIMULATIONS

Theoretical modeling of incubation times [16,15,23] starting at the molecular-level is all but impossible with

a twenty order of magnitude span between molecular motion time scales and those of disease onset. On the other hand, kinetic theory allows one to model long-time processes but ignores short distance spatial fluctuations, important in nucleation and growth. We have developed a lattice-based protein-level cellular-automata approach, which bridges these two methodologies [24]. Previously, we used it to calculate aggregation-time distributions, which compared favorably with the incubation-times inferred from BSE data [10,11]. We also showed that playing with the rules in such simple models can be a ‘cheap’ way to suggest, constrain and guide treatment protocols.

Our models consist of dilute concentrations of proteins diffusing on the lattice and interconverting between their properly folded state (PrP^c) and the misfolded state (PrP^{S^c}) [25]. Our key assumption is that the conformational state of a protein depends on the amount of water around it. A monomer isolated from others (surrounded by the omnipresent water) stays in its properly folded state. However, when proteins are surrounded by other proteins, thus excluding water from parts of their neighborhood, they can change conformations and go into a misfolded state (involving β sheet bonding). A key parameter of our model is the coordination, q_c , at which the misfolded conformation PrP^{S^c} becomes stable. Only misfolded monomers may remain stably in a cluster, possibly breaking away from a cluster when they fold back into the PrP^c form.

Assuming aggregation happens on the cell-surface, we choose a 2d hexagonal lattice. There is strong evidence that the local coordination environment of the sphingolipids to which the prion proteins attach is, in fact, hexagonal [26]. The lattice structure and the detailed protein motion are not crucial in our model. At each time step, proteins can move randomly by at most a unit lattice spacing. The magnitude of the time-step is set by the time for a single monomer to misfold. It is implicitly assumed that proteins co-adsorb with each other followed either by a conversion in shape or separation. It is this conversion process which sets the unit of time.

By playing with the cellular automata rules it is possible to get different aggregate morphologies and aggregation time distributions. First, we consider the case where proteins are isotropic objects. We have performed a large number of runs at values of $q_c = 1, 2$, and 3, with different monomer concentrations (held fixed during the simulation). The aggregation time is defined as the time required to grow from initial seed of size \mathcal{A}_i to a final size \mathcal{A} . The lower coordination rules effectively remove the nucleation barrier, leading to frequent nucleation of new clusters. Typical aggregate configurations (and stable seeds) are shown in Fig. 1.

From these studies, we see that lowering the critical coordination provides too rapid a growth for prion aggregates, and with no nucleation barrier at these concentrations. In contrast, for $q_c = 3$, the aggregation is

very slow and it is characterized by a broad incubation time distribution, with a clear separation in time-scales for seeded and unseeded (*i.e.* infectious and sporadic) cases.

We can also obtain one dimensional fibril growth by considering the proteins to be anisotropic. For example, on a square lattice, we can get fibrils by: (i) identifying a preferred bonding face to our simple point proteins, now made into squares. (ii) We choose a critical coordination of 2. (iii) We make edge bonding of proteins with adjacent preferred faces to be quite strong under coordination $q=1$ (*i.e.*, the conversion probability is higher than 50%), and somewhat less strong for face to face meeting of proteins. We assume zero conversion probabilities for all other faces. By choosing three kinds of faces with appropriate rules, we can obtain equivalent results on the hexagonal lattice. These rules assure fibril growth which is dimer dominated (see Fig. 1).

IV. STOCHASTIC ANALYSIS OF AGGREGATION

In the low concentration limit, the aggregation results from a sequential addition of proteins to the initial seed. However, addition of monomers is not always stable. Given the rules, various stages of the aggregate size and shape require a pair of proteins (a dimer) to arrive simultaneously, in order to attach in a stable manner. Thus, the entire process can be approximated by one of stochastic sequential addition of monomer and dimer units. As the concentration, c , goes to zero, the monomer addition rate is proportional to c , whereas the dimer addition rate is proportional to c^2 , and thus the growth will involve a minimum number of dimers and these will provide the dominant contribution to the growth times.

The growth to a final size \mathcal{A} from an initial size \mathcal{A}_i involves sequential addition of n units. The probability for the successive additions at intervals t_1, t_2, \dots, t_n is

$$P(t_1, t_2, \dots, t_n) = \prod_{j=1}^n p_j e^{-p_j t_j}, \quad (8)$$

where the rate for the j th unit, p_j , depends on the geometry of the aggregate and the kind of unit (monomer or dimer) to be added. Hence, the probability distribution associated with the total growth time is

$$P(t) = \int_0^\infty dt_1 \dots \int_0^\infty dt_n \prod_{j=1}^n p_j e^{-p_j t_j} \delta(t - \sum_{i=1}^n t_i). \quad (9)$$

This integral can be evaluated by standard methods for arbitrary p_i . We note the answers for two cases:

1) The attachment probabilities are identical for each unit *i.e.* $p_j = p$ for all j . In this case the probability distribution is the Gamma distribution:

$$P(t) = \frac{p(pt)^{n-1}}{(n-1)!} e^{-pt} \quad (10)$$

2) The rate, $p_j = p + jp'$, increases linearly with j . In this case we obtain the Beta distribution in e^{-t} [27]:

$$P(t) = A e^{-(p+p')t} (1 - e^{-p't})^{n-1} \quad (11)$$

In 1d fibril growth, dimers are attached one by one with the area available for attachment of dimers staying constant, and thus Eq. 10 applies. For 2d compact growth, slow dimer attachments have to be combined with rapid filling up of rows by monomers. In the low concentration limit, the rate is limited by dimer attachment probabilities which increase linearly with the number of dimers already attached, thus leading to Eq. 11.

At finite concentrations, the monomer attachment times can no longer be neglected, and a more accurate treatment of the time scales in the 2d case requires a convolution of probabilities for monomer attachment times with those for dimer attachment times. The geometrical counting of number of monomers and number of dimers needed to grow to the desired size is straightforward and can be used to develop accurate fits to the numerical data (See Figure 2 A).

An important aspect of our 2d model is the asymptotic compression of the distributions at low concentrations. The initial stage of the growth is extremely slow and the process speeds up significantly as the aggregate grows. Thus, the mean aggregation time, $t_m(1)$ to go from an initial seed \mathcal{A}_i to a final size \mathcal{A} can be much larger than the typical aggregate-doubling time t_2 to go from size $\mathcal{A}/2$ to \mathcal{A} . Fig. 3 shows the ratio $t_2(1)/t_m(1)$ for different concentrations and different final sizes \mathcal{A} . The crossover to monomer dominated behavior ($t_2/t_m(1) \approx \frac{1}{2}$) is indicated at the highest concentration whereas at low concentrations this ratio can be much smaller.

V. AGGREGATE-FISSIONING

Fissioning of aggregates leads to exponential growth as the fission products provide seeds for the next round of aggregation. In this subsection, we consider two mechanistic models of the fission process associated with either proteolytic cleavage of aggregates or mechanically induced breakage. We acknowledge that other models are possible.

We assume that the fission time is small compared to the aggregation time, and thus work in the limit of ‘instantaneous fission’ in which breakage of an aggregate happens much more rapidly than aggregation. This implies a narrow distribution of fission sizes peaked, say, at aggregate size \mathcal{A} , and in this limit our results are expected to be independent of the width of the fission distribution.

We consider two extreme limiting models of fission: (i) *Mechanical*. In this case, once the aggregate reaches fission size \mathcal{A} , it splits into two fragments of equal size $\mathcal{A}/2$. This should approximately describe the situation in which aggregate size is limited by nerve cell curvature (e.g., aggregation favors flat planar or linear structures, but the curvature of the neuron tends favors curved structures). (ii) *Physiological*. In this case, the aggregate can break into all smaller lengths at the fission scale. This mimics the outcome of protease attack for which there is no obvious preferred site for breakage.

Taking a fixed background concentration of monomers, which should be reasonable for at least short times in the disease. The kinetic equation for the time evolution of aggregates with size n (measuring the number of dimers present) and concentration $[a_n]$ is, for $n < \mathcal{A}$,

$$\frac{d[a_n]}{dt} = p_{n-1}[a_{n-1}] - p_n[a_n] + p_{f,n}[a_{\mathcal{A}}] \quad (12)$$

and, for $n = \mathcal{A}$,

$$\frac{d[a_{\mathcal{A}}]}{dt} = p_{\mathcal{A}-1}[a_{\mathcal{A}-1}] - p_{f,0}[a_{\mathcal{A}}] \quad (13)$$

Here, for 1d aggregation $p_n = p_0$, while for the 2d aggregation specified by our critical coordination three rules discussed in Sec. III, $p_n = p + np'$. For mechanical fission, $p_{f,n} = 2p_{f0}\delta_{n,\mathcal{A}/2}$, while for the physiological fission, $p_{f,n} = 2p_{f0}/(\mathcal{A} - 1)$. The instantaneous fission assumption requires $p_{f,0} \gg p, p'$.

We can identify the doubling time from Eqns. 12 and 13 by the following procedure: (i) Laplace transform the set of coupled equations to obtain a matrix equation in transform space; (ii) identify the largest positive eigenvalue of the Laplace matrix. In all cases, we find but one positive eigenvalue. We have systematically varied the fission size \mathcal{A} and studied the dependence of the exponential growth rate upon fission time. For fibrils, the mean time to aggregate to size \mathcal{A} is $t_m \approx \mathcal{A}/p$, while for the 2d aggregates, the mean aggregation time goes as $t_m \approx \ln(\mathcal{A})/p'$. In the one dimensional case, we find that for large \mathcal{A} , the doubling time t_2 tends to $0.5(0.43)t_m$ for mechanical(physiological) fission. Hence, there is but a factor of two difference between the aggregation time and the doubling time. Since the numerical difference between mechanical and physiological fission is not substantial, we have examined only the mechanical fission model for the 2d aggregate. In this case, we find that the largest eigenvalue of the Laplace matrix goes as $\simeq 0.4/p$ independent of \mathcal{A} , while the aggregation time scales as $\ln(\mathcal{A})/p'$. Hence, for sufficiently large \mathcal{A} it is possible to make $t_2/t_m \ll 1$.

These results have the attractive feature of linking the aggregation time, which we associate with the lag phase, to the doubling time in fission. However, we acknowledge that other processes may properly describe fission. In

particular, we cannot rule out continuous fissioning of fragments off of large aggregates which may lead to a very different result provided the fission rate is comparable to growth rates.

VI. DOSE-INCUBATION CURVE

In this section, we will look at the total incubation time and how it varies as a function of the inoculated dose using the aggregation-time distributions derived in the previous sections, and explore the extent to which it provides a quantitative description of experimental dose incubation curves. As discussed before, a key advantage of the 2D growth models is that, with a suitable fissioning scenario, they lead to lag times much larger than doubling times. This is difficult to accomplish with the 1D growth models. However, in this section we will assume that the doubling time is an independent free parameter. This allows us to fit the experimental dose incubation curves by both 1D and 2D models. The constraints on relative values of lag times and doubling times will be brought up in our discussions in the next section.

We now proceed to calculate the incubation time as a function of inoculated dose within our model for both 1d and 2d aggregation models and compare with laboratory data. Consider first the DIC of the 263K hamster scrapie strain. Kimberlin *et al* [28] have determined the DIC along with independent measurements of the doubling time t_2 and the final infectivity for this strain. The doubling time t_2 can also be inferred from the DIC in the region where it shows a logarithmic dose-dependence. Besides this experimental data, we need to know the clearance ratio r_i which gives the percentage of the number of infectious seeds in a given inoculum which are removed by rapid initial clearance. Let us illustrate this for the case of 1 LD₅₀ unit : in our model this corresponds to having a 50% probability of attaching a *single* infectious seed. Correspondingly the initial inoculum has to contain, on average, $\frac{50}{100-r_i}$ seeds (for $r_i > 50\%$, typical values from experiment are $r_i \sim 99\%$ [5]). We treat r_i as a parameter in our model to be determined by fitting the DIC. Using this, in conjunction with our results for the aggregation time distributions, we can generate theoretical DICs using the method outlined in Section II.

For a fixed aggregation size \mathcal{A} , probability of attachment p and infectivity ratio r_i , we then calculate the mean-square deviation (S^2) (normalized by the experimental error estimates for each data point) between the theoretical and experimental DICs. Minimizing S^2 gives us the optimal parameters, p and \mathcal{A} , for the particular strain for a given value of r_i within our model.

We consider first the DIC for the 263K hamster scrapie strain. In carrying out the fitting, we have ignored the results at the highest doses since in this limit we are approaching the saturation of the incubation time. For our

2d growth model, we get a good fit to the experimental data as indicated in Fig. 4a. The optimal parameters in this case are $\mathcal{A} = 16$ (with $\mathcal{A}_i = 10$), $p = 0.025 \text{ day}^{-1}$ and $r_i = 0$ (which seems unphysical) for which $S^2 \sim 0.07$. For a more realistic value of $r_i \sim 88\%$ we get $\mathcal{A} = 16$, $p = 0.16 \text{ day}^{-1}$ with $S^2 \sim 1.14$. From the fitting, one can see that the clearance ratio r_i cannot be much greater than $r_i \sim 88\%$ due to the constraints imposed by the experimental incubation and doubling times. It should be noted furthermore, that the above procedure does not uniquely determine these parameters since comparably good fits are obtained for higher values of \mathcal{A} by correspondingly adjusting p . For the 1-d growth model, we also get a good fit with $S^2 \sim 0.35$ for $\mathcal{A} = 8$ (with $\mathcal{A}_i = 4$) and $p = 0.11 \text{ day}^{-1}$.

One of the unusual features of the 263K scrapie strain in hamsters is that at high doses the lag-time is negligibly small. This feature is clearly seen in the time-course measurements [28] of infectivity and also accords with the theoretical best-fit results described above. In order to test our procedure for a more representative strain we have also obtained a fit for the experimental DIC for the ME7 strain in C57Bl mice [29]. The results obtained by using our 2d growth model are shown in Fig. 4b. In this case, the theoretical fit is not as good as that obtained for the 263K strain; the optimal parameters correspond to $\mathcal{A} = 140$, $p = 0.033 \text{ day}^{-1}$ for $r_i = 99$ which gives $S^2 \sim 3.75$. A comparably good fit was obtained by using the 1d growth model with the optimal parameters $\mathcal{A} = 40$, $p = 0.23 \text{ day}^{-1}$ for $r_i = 99$ which gave $S^2 \sim 5.02$. However in contrast with the 263K strain, the theoretical results for the ME7 strain give rise to a significant lag time of ~ 50 days for the highest dose inoculated. This is a testable prediction for time-course measurements of infectivity for the Me7 strain in C57Bl mice.

Finally, we have used the above procedure to analyze the Sc237 scrapie strain in hamsters. In many respects, this strain is similar to the 263K scrapie strain in hamsters, however an analysis of the respective DICs reveals some significant differences. Based on the theoretical best-fit formula for the DIC [3], we can estimate a doubling time t_2 for the Sc237 strain to be ~ 2.1 days whereas the doubling time for the 263K strain is ~ 3.9 days. This difference is also reflected in our theoretical best fit DIC curve for this strain which, for $r_i = 99$, is given by the parameters $\mathcal{A} = 80$ $p = 0.052 \text{ day}^{-1}$. For our 1d model the corresponding values are $\mathcal{A} = 62$, $p = 0.35 \text{ day}^{-1}$. Note that the experimental error estimates were not available for dose-incubation data for this strain, so we assumed them to be the same as that for the 263K strain in determining the best fit. Using the above fits, we see that the theoretical prediction for the mean lag-time for an inoculated dose of 1 LD₅₀ unit is ~ 50 days. This value seems to be in good agreement with the experimental results for low dose inoculations for this strain [3].

The key results from our fitting (using the 2d growth model) are summarized in Table I. Based on the above results, we conclude that while our model accounts for the features of the DIC and gives a good fit to the experimental data, the latter cannot be used to distinguish between the 1d and 2d growth morphologies or to ascertain the model parameters conclusively. However despite the ambiguity in the model parameters, there are some robust predictions we can make after fitting the DICs. We find that the experimental DIC, in conjunction with our model, can be used to make predictions for the time-course of infectivity: in particular we can predict the lag-time as a function of dose. While the duration of the lag-time that we calculate does depend on the clearance ratio r_i , we note that the trend is that increasing r_i reduces the lag-time. Thus by measuring the lag-time at high doses we can determine the parameter r_i in our model, which then yields testable predictions for the lag-time at low doses. In the case of the the Sc237 scrapie strain in hamsters, our calculated lag-time at low dose agrees well with experimental results for the same. For the other strains, the predictions for the lag-time at low dose are a key testable prediction of our model.

VII. CONNECTION TO EPIDEMIOLOGICAL DATA

We have found no dose incubation time data available for large mammals in the literature, so to gain insight we have analyzed epidemiological data for BSE in cattle [11], a tabulation of incubation times from iatrogenic CJD associated with *dura mater* transplants [38], and the cluster of five victims of vCJD from the village of Queniborough in the United Kingdom [39–41]. The goal is to produce approximate estimates of aggregate size and growth time scales for comparison to the small mammal data, and, potentially, to guide future epidemiological and public health studies.

In brief, our assumptions and methods are as follows:

- 1) *Model Distributions* We apply only the 2d model in the dilute dose limit (suitable for digested prions); comparable quality fits can be obtained from the 1d model, but the estimated t_2/t_m ratio consistently and strongly violates our mechanistic model result from Sec. V, while the bound for the 2d case is satisfied.
- 2) *Number of Doublings*. For mice and hamsters, with 1g brains, 30 doublings to incubation is typical. Given that the mean cattle brain is 500g, and the mean human brain 1500g, we take $n_2 = 40$ doublings from infection to incubation for cattle and humans.
- 3) *BSE fits*. Ref. [11] provides a candidate incubation time distribution which best fits the epidemic time course, and yields a mean incubation time $\langle t \rangle = 5$ years and standard deviation of 1.3 years. The width fixes p' uniquely for given $n, l = 1 + p'/p$, with p' weakly

dependent upon n . We readily calculate $t_m(n, l, p') \approx (\psi(n+l) - \psi(l))/p'$, and we take the difference $\langle t \rangle - t_m$ to be $n_2 t_2$, the length of the exponential growth phase. With a minimum $t_2 = 5$ days typical for hamsters and mice (see Table II), the maximum n value can be found at given l . For small aggregates, $n = 6$ is taken to be a plausible minimum value which bounds t_2 above as 15 days. The results for $l = 2, 10$ are summarized in Table II. Importantly, we find the maximum aggregate size at fission to be of order 80-100 monomers, approximately independent of l for $2 \leq l \leq 10$.

4) *Fits to iatrogenic CJD data.* The data of Ref. [38] sharply constrain the size of the aggregate at fission, since the ratio of standard deviation ($\simeq 3$ years) to mean ($\simeq 5.8$ years) rules out $n > 4$ for all $l = 1 + p'/p$ values. To fit the data we perform the following procedure: a) We produce a parameter free estimate of t_m by multiplying σ by the ratio of t_m/σ for a given choice of n, l ; this subtracted from $\langle t \rangle$ yields the estimated doubling phase period (and t_2 , assuming $n_2 = 40$ as above). (b) Using the estimated value of $n_2 t_2$, we produce a one parameter fit in p' to the cumulative distribution $F^{(1)}(t - n_2 t_2)$ for the given n, l choice. We find for $n = 3$, we can consistently fit for all l , while for $n = 4$, comparable quality fits are obtained for $l = 2, 3$, but for $l \geq 4$ $n = 4$ is no longer a viable choice. The resulting *robust* estimates of incubation parameters are $t_2 = 5.4 \pm 0.4$ years, $\sigma = 3.2 \pm 0.2$ years, and $t_2 = 7 \pm 1$ days. The attachment rates p' vary systematically with l , but are at most $0.22 \pm 0.042/\text{year}$. (Error bars reflect 95% confidence intervals.)

5) *Fits to Queniborough vCJD incubation time data.* For vCJD, we have extracted an estimated onset time distribution from the Queniborough cluster, taken as incubation times, from the available scientific and journalistic literature [39–41]. We assume that this is a single dose event, in the low dose limit. We determine the estimated mean $\langle t \rangle$ from the five data points to be Feb., 1998. Using non-linear least squares analysis, we fit the cluster data to the cumulative beta distribution $F^{(1)}(t - \langle t \rangle + t_m(n, l, p'))$, placing points at half steps of probability increment. We also estimated the upper and lower bounds to p' corresponding to 95% confidence, which yields a corresponding range for t_m, σ . Unlike the iatrogenic CJD and BSE data, the overall incubation time is unknown, which prohibits an estimate of t_2 . We thus take a reasonable estimate for the maximum doubling time at $t_2^{max} \leq 30$ days. Using the minimum estimate of 9.0 years for the incubation time from epidemiological studies [32], we thus estimate a minimum lag time of $t_m^{min} = t_{inc}^{min} - n_2 t_2^{max} = 5.7$ years. The minimum aggregate size at fission which can exceed this t_m^{min} value at the upper 95% confidence limit is $n = 4, l = 2$ (16 monomers). We can take the upper aggregation size limit from BSE as a reasonable bound ($n = 20, l = 2$ or $n = 10, l = 10$ giving 80 monomers). We summarize our results in Table III, for two values of l . We stress that our

results here are at best a crude guide to expected model fits since: (1) there are only five data points to fit to and several model parameters, (2) the infection is likely to be characterized by slow *heterologous* protein attachment for short times and more rapid *homologous* attachment for long times, while we assume a single effective attachment probability, and (3) there is no guarantee that the postulated single event was in the low dose limit.

Given the simplicity of our model and the assumptions made for fitting, we shall emphasize the most robust results of our analysis. Our results are summarized in Tables II (BSE), III (vCJD). We find several robust features: (i) For BSE, iatrogenic CJD, and vCJD, we find that a wide range of l produce comparable fits, corresponding to a different starting seed size. We have thus quoted values from $l = 2$ and $l = 10$, the former representing nearly minimal seed sizes, the latter maximal plausible ones. (ii) In all three cases, the standard deviation of the incubation time distribution is large (1.2 years for BSE, vCJD, and 3.2 years for iatrogenic CJD), supporting the assumption of small dose. (iii) The attachment rates are all comparable (BSE: 0.6/yr; iatrogenic CJD: $\leq 0.2/\text{year}$; vCJD: $\leq 0.66/\text{yr}$) and are significantly smaller than for the small mammal analysis of the previous section ($\geq 11/\text{year}$ from Table I). (iv) For BSE and CJD, t_2 is comparable to values for small mammals (eg., ≤ 15 days for BSE, 8 days for iatrogenic CJD). For all strains considered here with the exception of 263K for hamsters, ratios of t_2/t_m are small. We shall discuss the large t_2 values for vCJD below. (v) Aggregate sizes are comparable for large and small mammals ($\leq 80 - 100$ monomers for BSE, for iatrogenic CJD with $l = 2, n = 3$ we get 16 monomers, and for vCJD apparently tens of monomers also), compared with 16-360 for the small mammals of Table I. Hence in each case, given a 2 nm characteristic protein size, the length scale is of order tens of nanometers. (If the aggregating entities are in fact oligomers as suggested by Ref. [26], we only double the length scale.)

Hence, our analysis strongly suggests interspecies variation in incubation times is dominated by t_m , given similar doubling times and aggregate sizes. In our model, variation in t_m is governed by p' , which then suggests a significantly higher homeostatic monomer concentration in small mammals compared to large ones, a point we discuss further below.

Our fitting of the Queniborough data also suggests that long (≥ 20 years) incubation times for vCJD are implausible. The maximum t_m value found (at the upper 95% confidence limit) for $n = l = 10$ is 9.3 years; even with the extreme $t_2 = 30$ day value, this gives a 12 year incubation time. We note that the most probable (best fit) p' values yield larger and implausible t_2 values for the minimum epidemiological estimate of the incubation time. To the extent our model is applicable, this implies

9 years likely overestimates the incubation period. In consequence, in conjunction with epidemiological analyses, our work suggest that the number of vCJD infections is likely to number in the hundreds.

VIII. DISCUSSION

Recall that our basic hypothesis is that incubation times are controlled by prion-aggregation around infectious external seeds on the neuronal surface. Furthermore, in our calculations, the distribution of aggregation times arises from the stochastic growth process from seeds of a given initial size. That only a narrow range of seed sizes is relevant here maybe motivated by size-sensitivity of (a) the blood-brain barrier (b) attachment probability and (c) transportability of the seeds. The lag phase corresponds to growth from initial seeds to a characteristic fissioning dimension \mathcal{A} , after which one gets a multiplication in seeding-centers and an exponential growth in infectivity.

That there is a long lag time despite external seeding by intracerebral inoculation [5,8], and a doubling time which is typically significantly shorter [5], both of which become sharply defined at high doses, seems to be a general feature of the prion diseases. Our 2d compact aggregate model, with the assumptions of the preceding paragraph, explains these facts. In particular, 2d compact aggregation generates a broad distribution of aggregation times for a single seed with a well defined sharp onset time (t_0) and mean aggregation time ($t_m(1)$). With increasing number of seeds (D_i), the distribution of times for the first seed to reach the typical fissioning size \mathcal{A} will narrow. Correspondingly the lag time, determined by the first fissioning event, will become sharply defined and concentrate at the onset time, which only weakly depends upon D_i .

The doubling time (t_2) is defined by fissioning and subsequent growth from size $\mathcal{A}/2$ to \mathcal{A} . Since growth from different seeds is independent, self-averaging ('law of large numbers') gives a sharply defined t_2 . Thus at high doses both the lag time and doubling time are sharply defined which accounts for one of the most striking features of prion diseases: the reproducibility of incubation times at high doses. Indeed, we can explain several features of the dose-incubation curve. Notably, above a saturation dose D_s , the incubation time does not decrease, while for $D < D_s$, the incubation time varies as $\log(D)$, showing deviations from the log only below a much smaller value D_{min} [2,17]. The total incubation time is the sum of the lag time and $n_d t_2$, where n_d is the number of doubling steps. Assuming that the onset of clinical symptoms is related to the damage of a fixed number of neurons [16], the logarithmic dose dependence of the number of doubling steps follows from the fact that number of seeds grows exponentially in the fissioning stage. In the range

$D_{min} < D < D_s$, the lag time does not change appreciably with dose, thereby giving rise to the logarithmic dose-dependence of the incubation time in this range. At low doses ($D < D_{min}$), the lag-time increases towards $t_m(1)$ (the mean aggregation time for a single seed) giving rise to a broad distribution of incubation times and the deviation from the logarithmic behavior in the DIC which is observed experimentally. [22]

Furthermore, we note that in our mechanistic fissioning model, the doubling time (t_2) is bounded above by the time to grow from size $\mathcal{A}/2$ to \mathcal{A} . If the fission produces jagged fragments, these can be effectively filled by monomers which will accelerate the subsequent growth process. This is only possible for 2d compact aggregates and not for 1d fibrils, for which the exposed ends will always be limited to dimer growth. This possibility may account for the effective '1/c' dependence in the incubation time observed for transgenic hamsters with multiple copies of the prion gene [30], noting that for hamsters the doubling phase appears to dominate incubation [28].

A key difference between the 1d and 2d morphology (shown in section IV) is that, within our model, in case of the latter (i) the lag-time can be an order of magnitude larger than the doubling time. If the total time in doubling-steps becomes large compared to the lag time, the overall distribution will be relatively narrow. Thus, only in the case of 2d growth can one get (ii) a wide distribution for the overall incubation time, with a width comparable to the mean. Thus assuming (i)-(ii) to result entirely from the growth processes discussed here, strongly points to a 2d (or 3d) morphology as controlling the incubation times.

The early growth morphology clearly deserves further experimental attention [31,34]. Typically, the *in vitro* morphology of prion aggregates has been found to be fibrillar [35]. Frequently large fibrillar aggregates are also observed post mortem in brain tissues. The morphology and size scale for aggregates that cause neuronal death and infection is not known. One could argue that the reason why *in vitro* aggregates are not infectious is because they do not have the proper morphology. We speculate that the attachment to lipid membranes could make a vital difference to the aggregation process, which is missing in *in vitro* experiments. It would be very interesting to carry out the *in vitro* studies of prion aggregation in presence of lipid membranes.

An important byproduct of our analysis is the ability to predict the time course of infectivity from the DIC. Provided we take the doubling time (t_d) as an independent experimental parameter, such predictions are very robust and do not rely on many details of the aggregation-fissioning model, including initial growth morphologies. Such predictions are particularly significant since experiments which measure the time-course of infectivity, and hence determine the lag phase, are extremely expensive and time consuming. This dose dependence of the lag

phase may well be a significant factor in assessing the risk of infection.

Our results indicate that we can *infer* the (average) time-course of infectivity using the information supplied by the experimental DIC. Thus, based on our fits to the experimental DIC, we have made testable predictions for the time-course of infectivity, and in particular the lag time, as a function of dose. These predictions are in good agreement with the existing experimental results and their further experimental validation would prove very useful.

A factor which significantly affects the lag time is the probability of dimer attachment p ; lowering p increases the lag time. This is relevant in understanding the species barrier effect in which there is a reduction of incubation times with multiple passages in inter-species infection [36]. During first passage, the attachment of dimers is initially non-homologous but as the seed size increases it should change to homologous attachment. Since the non-homologous attachment probability should be smaller [37], the lag phase should be longer for first passage as compared to subsequent passages. Thus, in our picture, most of the difference in incubation times should come from the lag phase and the exponential growth phase should be similar between first and second passages. This has been observed experimentally for hamster scrapie passaged in mice [13]. We note that the estimated dimer attachment rates for mice and hamsters range from 9-60 per year (c.f. Table I), while for humans and cattle they are *maximally* 0.6 per year.

Furthermore, we observe that the estimated aggregate sizes are comparable between large animals (humans and cattle) and small animals, all in the ballpark of tens of nm, which is precisely the estimated size of the lipid rafts on which prions are hypothesized to rest [42]. The comparable sizes of aggregates at fission we find in our model between small and large mammals strongly suggests that the primary determinant of lag time is the dimer attachment rate which is regulated primarily by the concentration (for a given strain). This leads us to speculate that the concentration of normal prion proteins must vary dramatically between large and small species, which naturally leads us to envision a link to metabolic rate. Such a link is plausible if prion proteins play a functional role in relieving oxidative stress as has been proposed elsewhere [43]. The hypothesis of enhanced homeostatic PrP^c concentration in small animals relative to large ones is testable by direct examination of the brains of uninfected animals.

Finally, as noted in the preceding section, our model analysis yields 12 years as an extreme upper bound on the vCJD incubation time. We actually get reasonable doubling times only when we assume a total incubation below 9 years, which is the lowest epidemiological estimates. The important suggestion from this analysis is that the vCJD cumulative infection toll is likely to be

several hundred, vs. several hundred thousand [32].

Acknowledgements. We acknowledge useful discussions with F. Cohen. We thank D.D. Cox for a critical reading and discussion of our fit to the Queniborough data. R.V.K. and D.L.C. acknowledge support from the U.S. Department of Energy, Office of Basic Energy Sciences, Division of Materials Research. A.S. is supported by Sandia which is a multiprogram laboratory operated by Sandia Corporation, a Lockheed Martin company, for the United States Department of Energy under Contract No. DE-AC04-94AL85000. R.R.P.S. and D.L.C. have benefited from discussions at workshops of the Institute for Complex Adaptive Matter. We are grateful for a grant of supercomputer time from the Lawrence Livermore National Laboratory.

-
- [1] Prusiner, S.B., Gajdusek, D.C. and Alpers, M.P. *Ann. Neurol.* **12**, 1-9
 - [2] Prusiner, S.B., Cochran, S.P., Groth, D.F., Downey, D.E., Bowman, K.A. & Martinez H.M. *Ann. Neurol.* **11**, 353-358
 - [3] Prusiner, S.B., Tremblay, P., Safar, J., Torchia, M. & DeArmond, S.J. (1999), in *Prion Biology and Diseases*, ed. S.B. Prusiner (Cold Spring Harbor Laboratory Press, Cold Spring Harbor NY, 1999), p. 113-145
 - [4] Dickinson, A.G. & Outram, G.W. (1979), in *Slow transmissible diseases of the nervous system*, ed. S.B. Prusiner & W.J. Hadlow (Academic Press, New York, 1979), Vol. 2, p. 13-32.
 - [5] Manuelidis, L. & Fritch, W. (1996) *Virology* **215**, 46-59
 - [6] Bolton, D. C. (1998) *J. Gen. Virol.* **79** 2557-2562
 - [7] Beekes, M., Baldauf, E. & Diringner H. (1996) *J. Gen. Vir.* **77**, 1925-1930
 - [8] Kimberlin, R.H. & Walker C.A. (1988) in *Novel infectious agents and the central nervous system* Wiley, Chichester (Ciba Foundation Symposium 135), p. 37-62
 - [9] Mclean, A.R. & Bostock, C.J. *Phil. Trans. R. Soc. Lond. B* (2000) **355**, 1043-1050
 - [10] Stekel, D.J., Nowak, M.A. & Southwood, T.R.E. (1996) *Nature* (London) **381**, 119-119
 - [11] Anderson, R.M., *et al.* (1996) *Nature*, **382**, 779-788.
 - [12] Kimberlin, R.H. & Walker, C. A. (1977) *J. Gen. Virol.* **34**, 295-304
 - [13] Kimberlin, R.H. & Walker C.A. (1978) *J. Gen. Virol.* **42**, 107-117
 - [14] Post, K., Brown D.R., Groschup, M., Kretzschmar, H.A. & Riesner, D. (2000) *Arch. Virol.* (Suppl.) **16**, S265-S273
 - [15] Eigen, M. (1996) *Biophys. Chem.* **63**, A1-A18.
 - [16] Nowak, M.A., Krakauer, D.C., Klug, A. & May R.M. (1998) *Integr. Biol.* **1**, 3-15.
 - [17] Masel, J., Jansen V.A.A. & Nowak M.A. (1999) *Biophys. Chem.* **77**, 139-152.
 - [18] Masel J. & Jansen V.A.A. (2000) *Biophys. Chem.* **88**, 47-59.

- [19] Payne R.J.H. & Krakauer D.C. (1998) *Proc. Roy. Soc. Lond. B.* **265**, 2341-2346.
- [20] Stumpf M.P.H. & Krakauer D.C. (2000) *Proc. Nat. Acad. Sc. USA* **97**, 10573-10577.
- [21] Kellershohn N. & Laurent M. (2001) *Biophys. Jour.* **81** 2517-2529.
- [22] Prusiner, S.B., Groth, D.F., Cochran, S.P., Masiar, F.R., McKinley, M.P., Martinez, H.M. (1980) *Biochemistry* **19** 4883-4891.
- [23] Harper, J.D. & Lansbury Jr., P.T. (1997) *Ann. Rev. Biochem.* **66**, 385-407
- [24] Slepoy, A., Singh, R.R.P., Pazmandi, F., Kulkarni, R. V. & Cox, D.L. (2001) *Phys. Rev. Lett.* **87**, 058101
- [25] Cohen, F.E. & Prusiner, S.B. (1998) *Ann. Rev. Biochem.* **67** 793-819
- [26] Wille, H., Michelitsch, M.D., Guenebaut, V., Supattapone, S., Serban A., Cohen, F.E., Agard, D.A. & Prusiner, S.B. (2002) *Proc. Nat. Acad. Sc. USA* **99**, 3563-3568.
- [27] Szabo, A. (1988) *J. Mol. Biol.* **199**, 539-542
- [28] Kimberlin, R.H. & Walker C.A. (1986) *J. Gen. Virol.* **67**, 255-263.
- [29] Taylor, D. M., McConnell, I. & Ferguson, C. E. (2000) *Jour. of Virol. Meth.* **86** 35-40
- [30] Prusiner, S.B., Scott M., Foster D., Pan K.-M., Groth D., Miranda C., Torchia M., Yang S.-L., Serban D., Carlson G.A., Hoppe P.C., Westaway D., and DeArmond S.J. (1990) *Cell* **63**, 673-686
- [31] Horiuchi, M. & Caughey, B. (1999) *Structure with Folding and Design* **7**, R231-R240.
- [32] Ghani, A.C., Ferguson, N.M., Donnelly, C.M., Anderson, R.M., (2001) *Nature* **406**, 583-584; Valleron, A.-J., Boelle, P.-Y., Will, R., Cesbron, J.-Y. (2001) *Science* **294**, 1726-1728; Huillard d'Aignaux, J.N., Cousens, S.N., Smith, P.G. (2001) *Science* **294**, 1729-1731.
- [33] Ferguson, N.M., Donnelly, C.M., Woolhouse, M.E.J., Anderson, R.M. (1998) *Phil. Trans. Ser. B R. Soc. London* **352**, 803-838.
- [34] Rochet, J.C. & Lansbury P.T. (2000) *Curr. Op. Struc. Biol.* **10**, 60-68
- [35] Ionescu-Zanetti, C., Khurana, R., Gillespie, J.R., Petrick, J.S, Trabachino, L.C., Minert, L.J., Carter, S.A. & Fink A.L. (1999) *Proc. Nat. Acad. Sc. USA* **96**, 13175-13179.
- [36] Lasmézas, C.I., Deslys, J.-P., Robain, O., Jaegly, A., Beringue, V., Peyrin, J.-M., Fournier, J.-G., Hauw, J.-J., Rossier J. & Dormont D. (1997) *Science* **275**, 402-404.
- [37] Horiuchi, M., Priola, S.A., Chabry, J. & Caughey, B. (2000) *Proc. Natl. Acad. Sci. USA* **97**, 5836-5841
- [38] Lang, C.J.G., Heckmann, J.G., Neundörfer, (1998) *J. Neurol. Sci.* **160** 128-139.
- [39] The five deaths were: August 1998, October 1998 (2), May 2000, October 2000, and from the scientific and journalistic literature we have inferred that the observed onset dates were: August 1996, September 1997, October 1997, and Jan 1999 (2). There is a four month uncertainty about one of the latter onset times. For a report, see <http://www.leics-ha.org.uk/cjd.htm> and <http://www.rense.com/general4/cluster.htm>.
- [40] Stecklow, S., (June 12, 2001) *Wall St. Journal* p. A1.
- [41] Allroggen, H., Dennis, G., Abbott, R.J., Pye, I.F., (2000) *J. Neurol. Neurosurg. Psychiatry* **68**, 375-378.
- [42] Simons, K., Toomre, D. (2000) *Nature Reviews Mol. Cell Biol.* **1**, 31-39.
- [43] Guentchev, M., Siedlak, S.L., Jarius, C., Tagliavini, F., Castellani, R.J., Perry, G., Smith, M.A., Budka, H. (2002) *Neurobiology of Disease* **9**, 275-281; Milhavel, O., Lehmann, S. (2002), *Brain Res. Rev.* **38**, 328-339; Brown, D.R. (2001), *Trends. Neurosci.* **24**, 85-90.

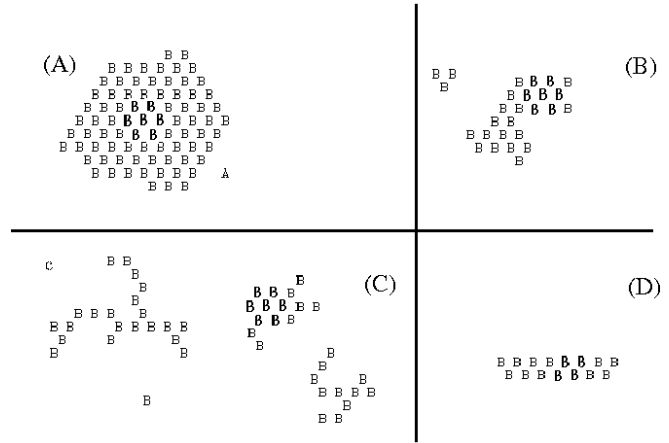


FIG. 1. Morphologies of seeds (bold Bs) and corresponding aggregates due to the different rules: (A) $q_c = 3$, (B) $q_c = 2$, (C) $q_c = 1$ and (D) fibril growth (see text)

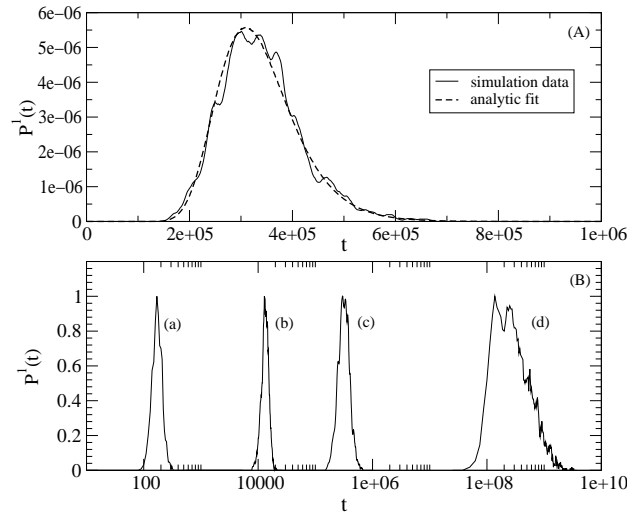


FIG. 2. (A) Comparison of simulation data for single seed aggregation ($\mathcal{A}_i = 10$, $\mathcal{A} = 80$, $c = 0.2\%$) and fit using analytical calculations (see text) for 2d growth with $q_c=3$. The unit of time is 1 simulation sweep. (B) Probability distributions for (a) $q_c = 1$, (b) $q_c=2$, (c) $q_c=3$ and (d) sporadic with $q_c=3$ at the same concentration ($c = 0.2\%$). The maximum probability for all distributions is scaled to unity. The sporadic result is obtained by scaling the data at $c = 1\%$ with an empirically determined c^{-3} factor.

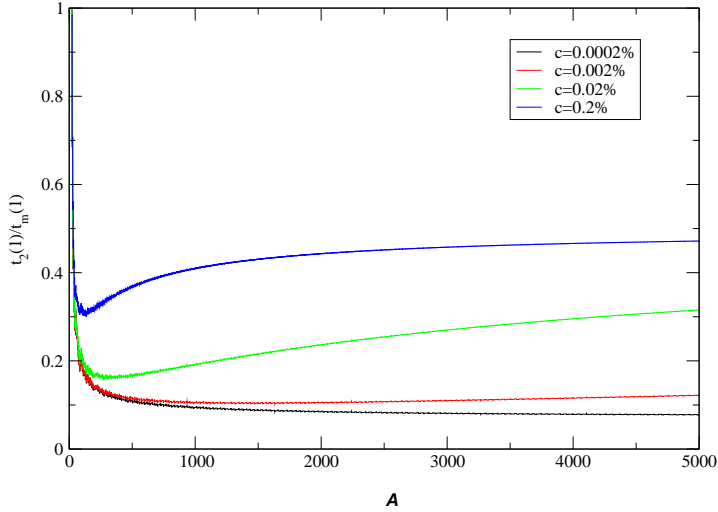


FIG. 3. Ratio of characteristic doubling time (t_2) to mean incubation time (t_m) as a function of fissioning size \mathcal{A} for single seed growth in 2d for different monomer concentrations, showing asymptotic compression as $c \rightarrow 0$.

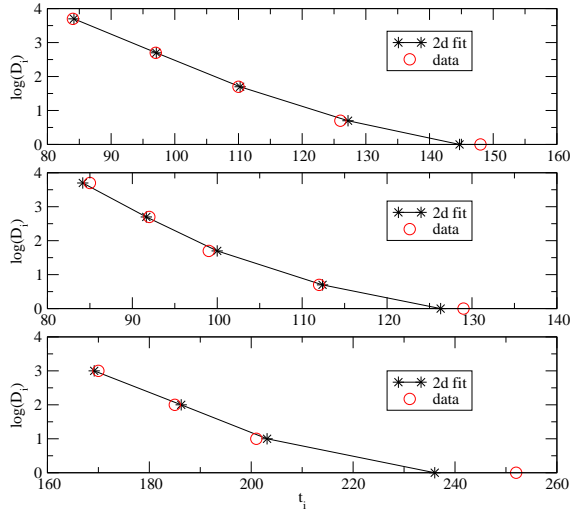


FIG. 4. (A) Experimental and theoretical dose-incubation curves for the 263K hamster scrapie strain for $r_i = 0$. The x-axis shows the incubation time and the y-axis shows the logarithm of the number of seeds inoculated. The theoretical curve is the best fit to the experimental data using the 2d growth model for aggregation. (B) Same as A but for the Sc237 strain in hamsters with $r_i = 88$ (C) Same as A but for the Me7 strain in C57Bl mice with $r_i = 88$

TABLE I. Calculated best-fit parameters and predictions for low dose lag times for 3 scrapie strains. ^a Ref. 28. ^b Ref. 3. ^c Ref. 29.

Strain	t_2 (days)	r_i	Lag time (days)	p' (days ⁻¹)	\mathcal{A}	S^2
263K	3.9 ^a	0	27.7	0.025	16	0.07
		88	4.3	0.16	16	1.14
Sc237	2.1 ^b	88	56.9	0.052	140	0.11
		99	48.9	0.052	80	0.11
Me7	4.5 ^c	88	107	0.033	360	3.86
		99	89.6	0.033	140	3.75

TABLE II. Fits to incubation time distribution for BSE (Refs.[11,33]).

l	n	p' (yrs ⁻¹)	t_m (yrs.)	t_2 (days)
2	6	0.57	2.8	20
2	23	0.61	4.5	5
10	6	0.15	3.2	16

TABLE III. Fits to onset time distribution from Queniborough cluster (refs. 39-41). Here $l = 1 + p/p'$. Doubling times are computed for best fit t_m , values, and the upper and lower quotes for p', t_m, σ represent 95% confidence intervals. t_2 values are only quoted for best fit p' .

l	n	p' (yrs ⁻¹)	$t_m(t_m^{(+)}, t_m^{(-)})$ (yrs)	$\sigma(\sigma^{(-)}, \sigma^{(+)})$ (yrs)	t_2 (days)
2	4	0.55(0.21,0.89)	2.3(1.4,5.4)	1.2(0.8,3.2)	61
2	20	0.64(0.25,1.07)	4.1(2.5,10.6)	1.2(0.7,3.1)	45
10	6	0.17(0.27,0.067)	2.9(1.8,7.3)	1.2(0.7,3.1)	56
10	10	0.20(0.077,0.32)	3.6(2.2,9.3)	1.2(0.7,3.1)	37